Journal of Magnetic Resonance 207 (2010) 140–148

Contents lists available at ScienceDirect

Journal of Magnetic Resonance

journal homepage: www.elsevier.com/locate/jmr

On the choice of heteronuclear dipolar decoupling scheme in solid-state NMR

Subhradip Paul [a], N.D. Kurur [b], P.K. Madhu [a,*]

[a] Department of Chemical Sciences, Tata Institute of Fundamental Research, Homi Bhabha Road, Colaba, Mumbai 400 005, India
[b] Department of Chemistry, Indian Institute of Technology Delhi, Hauz Khas, New Delhi 110 016, India

ARTICLE INFO

Article history:
Received 27 July 2010
Available online 9 September 2010

Keywords:
Solid-state NMR
Heteronuclear dipolar decoupling
Magic-angle spinning
TPPM
SPINAL
PISSARRO
SW_f-TPPM
Rotary resonance
High-phase TPPM

ABSTRACT

We present here a comparison of different heteronuclear dipolar decoupling sequences at the moderate magic-angle spinning (MAS) frequency (ν_r) of 30 kHz. The radio-frequency (RF) amplitude (ν_1) ranges from the low power ($\nu_1 < \nu_r$) to the high power regime ($\nu_1 > 2\nu_r$) and includes the rotary resonance conditions ($\nu_1 = n\nu_r$) where $n = 1, 2$. For decoupling at the rotary resonance condition, we recently introduced a modification of TPPM, namely high-phase TPPM, whose properties will be discussed here. Finally, based on earlier published and current experimental results we suggest the optimal sequence for heteronuclear dipolar decoupling at any RF amplitude and MAS frequencies up to 35 kHz.

1. Introduction

Efficient heteronuclear dipolar decoupling is an absolute necessity in order to achieve high-resolution spectra of rare nuclei like ^{13}C and ^{15}N. A combination of magic-angle spinning (MAS) and efficient radio-frequency (RF) pulse schemes is required to remove the heteronuclear dipolar couplings between the rare nuclei and the abundant spins like ^{1}H. Initially continuous-wave (CW) irradiation of high power was used for decoupling [1]. With the introduction of two-pulse phase modulation (TPPM) by Bennett et al. [2], the decoupling sequences shifted towards the use of multiple pulse sequences with modulations in phase, frequency, and/or amplitude as they led to improved sensitivity and/or resolution over the CW scheme. Investigation into the mechanism of the TPPM scheme led to modification of the sequence to include frequency modulation in combination with phase modulation (FMPM) [3] and amplitude modulation (AMPM) [4]. Fung and coworkers introduced a sequence called SPINAL [5] which involves incremental alteration of the phase of four TPPM units. Supercycled version of SPINAL, namely SPINAL-64, was later introduced [6], which has found a wide range of applications. Recently, another version of TPPM was introduced which involves an adiabatic sweep of the pulse length in eleven pulse pairs of TPPM [7]. This version of TPPM is called SW_f-TPPM. Variants of SW_f-TPPM and SPINAL also were introduced recently [8,9]. Comparison with other heteronuclear dipolar decoupling schemes has shown SW_f-TPPM to be better in terms of sensitivity or robustness when experimental parameters like the flip angle, offset, and/or MAS frequency are varied [7,10–13].

With the advent of MAS probes that can spin at frequencies up to 80 kHz, the search for decoupling schemes at high MAS frequencies has gained utmost importance. With the aim of increasing the sensitivity of NMR, high magnetic fields have become necessary for big molecules. Increased field strengths lead to an increase in the size of the chemical-shift anisotropy (CSA) tensor, which in turn requires high spinning frequency to remove sidebands in the spectra arising from the incomplete averaging of the CSA interactions. Although fast MAS has the unique advantage of yielding high-resolution spectra of large molecules, conventional decoupling which requires very high radio-frequency (RF) amplitudes are unsuitable for molecules like proteins as they might degrade the samples. In addition, the high power puts considerable strain on the hardware. Hence, the use of low power decoupling schemes is an area of investigation. Recently Ernst et al. explored low power decoupling using CW and XiX schemes [14,15] whilst Ishii et al. have also demonstrated that TPPM, with a nutation frequency (ν_1) of $\nu_r/2$ or less provides efficient decoupling at high MAS frequency of 65 kHz [16].

One problem with the application of the conventional decoupling sequences to be applied at an RF amplitude level larger than twice the MAS frequency is the presence of rotary resonance (RR) conditions [17]. They occur when the decoupler nutation

* Corresponding author. Fax: +91 22 2280 4610.
E-mail address: madhu@tifr.res.in (P.K. Madhu).

1090-7807/$ - see front matter © 2010 Elsevier Inc. All rights reserved.
doi:10.1016/j.jmr.2010.08.023

frequency (ν_1) becomes integral multiples of the MAS frequency (ν_r) ($\nu_1 = n\nu_r$), where $n = 1,2,3,\ldots$. The RR condition occurs due to the interference between the physical rotation of the sample and the nutation induced on the spins by the RF field [17]. At these conditions, recoupling of the heteronuclear dipolar coupling occurs between the abundant spins and the rare spins leading to broadening of the peaks in the spectrum even in the presence of a heteronuclear dipolar decoupling sequence. The RR conditions with $n > 2$ are less pronounced and hence attention is focussed only on the $n = 1$ and $n = 2$ conditions here. PISSARRO is a recently introduced decoupling sequence which delivers superior performance at the RR conditions, where other conventional decoupling schemes fail to work [18]. Recently we have introduced a modified version of TPPM for heteronuclear decoupling at the $n = 1$ and $n = 2$ RR conditions [19].

We present here a comparison of CW, TPPM, SW$_f$-TPPM, XiX, PISSARRO, SPINAL-64 and high-phase TPPM, over a wide range of power levels (5–90 kHz) at a moderate spinning frequency of 30 kHz. The spinning frequency was chosen to allow comparison of the different sequences at both high and low ν_1. The range of RF chosen also brings the RR conditions into picture where it is shown that all the sequences except PISSARRO and high-phase TPPM fail. Results from both simulations and experiments are presented on the quenching of rotary resonances by PISSARRO and high-phase TPPM. We also study the properties of high-phase TPPM to understand its working and experimental optimisation.

2. Experimental

The experiments were carried out on Bruker AVI 500 MHz and AVIII 700 MHz spectrometers using 2.5 mm double- and triple-resonance probes respectively on commercially available U-^{13}C-glycine and U-^{13}C-L-histidine·HCl·H$_2$O. Nutation experiments were performed on a sample of commercially available adamantane to calibrate the RF amplitudes on the protons and the carbons.

3. Results and discussions

3.1. Comparison of decoupling sequences

In conventional high power decoupling at low to moderate MAS frequencies, the main averaging of the spin interactions is done by the RF pulses followed by MAS. In the regime of low power decoupling under fast MAS, the averaging processes are assumed to be reversed. The Hamiltonian is first averaged by the MAS while the weak RF power does the truncation of the higher-order terms of the time-averaged Hamiltonian [20]. It has been observed that the RF power needed for low power decoupling should be less than two times the spinning frequency [16]. Here, we focus on the decoupling efficiency of different heteronuclear sequences from ν_1 = 5–90 kHz including the rotary resonance conditions at a MAS frequency of 30 kHz.

We first focus on the decoupling at an RF amplitude range which is less than or equal to the MAS frequency ($\nu_1 \leqslant 30$ kHz). Fig. 1 shows the decoupling efficiency of six different sequences, SW$_f$-TPPM, TPPM, SPINAL-64, PISSARRO, XiX, and CW. The intensity of the $^{13}CH_2$ resonance of glycine is monitored as a function of the RF amplitude (ν_1). The pulse length optimisation of each sequence was performed as follows:

(a) SW$_f$-TPPM, TPPM, and SPINAL-64: The pulse length was varied in the range corresponding to a flip-angle of 150–220° and optimised for both TPPM and SPINAL-64 whilst for SW$_f$-TPPM, the optimal length was found to be close to a length corresponding to a flip angle of 180°.

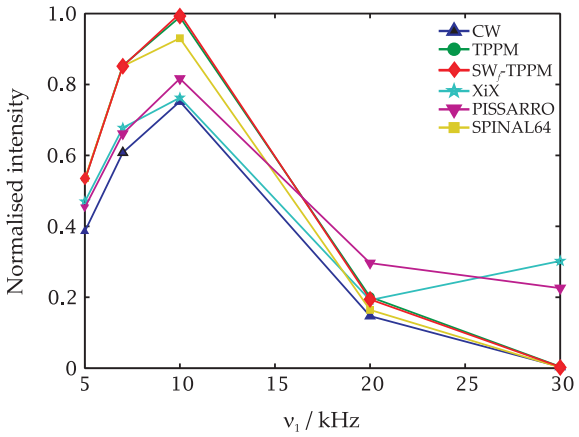

Fig. 1. Intensity comparison of CW, TPPM, SW$_f$-TPPM, XiX, SPINAL-64, and PISSARRO as a function of RF amplitude (5 kHz $\leqslant \nu_1 \leqslant$ 30 kHz) at a spinning frequency of 30 kHz. The normalised intensity of the $^{13}CH_2$ peak of a U-^{13}C-glycine sample is plotted. The normalisation was done with respect to the best intensity obtained which is with SW$_f$-TPPM at RF amplitude ν_1 = 10 kHz.

(b) PISSARRO and XiX: The optimisation of pulse length for PISSARRO and XiX follows two regimes of RF amplitudes:
- $\nu_1 < \nu_r$: The optimum decoupling is achieved when the pulse length is such that the flip angle lies in the vicinity of integer multiples of 360°($\nu_1\tau_p = k2\pi$) [15,21]. For optimisation purpose the pulse was varied corresponding to a variation of 50° on either side of the 360° pulse.
- $\nu_1 = \nu_r$: The pulse length was varied in the range of $0.1\tau_r$ to $3\tau_r$ and the optimal pulse length for PISSARRO is observed to be $\tau_p = 0.21\tau_r$. With this, XiX at the rotary resonance condition gives comparable decoupling performance as that of PISSARRO. This result is not surprising as the PISSARRO sequence can be derived by supercycling the basic unit of XiX.

From Fig. 1, the best decoupling in the low power regime is found to be at ν_1 = 10 kHz. SW$_f$-TPPM and TPPM yield the best result, followed by SPINAL-64, PISSARRO, XiX, and CW.

Fig. 2. shows the decoupling efficiency of the different sequences over the RF amplitude range 10 kHz $\leqslant \nu_1 \leqslant$ 90 kHz. The left panel shows the data at 500 MHz (^{1}H resonance frequency) and the right panel shows the data at 700 MHz (^{1}H resonance frequency). The pulse length optimisation was done as follows:

(i) SW$_f$-TPPM, TPPM, and SPINAL-64: The pulse length was varied in the range corresponding to a flip-angle of 150–220° and optimised for both TPPM and SPINAL-64 whilst for SW$_f$-TPPM, the optimal length was found to be close to a length corresponding to a flip angle of 180°.

(ii) PISSARRO: There are three different RF regimes for PISSARRO in which the pulse length needs to be optimised. In all these cases the pulse length was varied in the range of $0.1\tau_r$ to $3\tau_r$. The optimal pulse lengths are as follows:
- $\nu_r < \nu_1 < 2\nu_r$: The optimum pulse length was found to be $\tau_p \approx 0.3\tau_r$.
- $\nu_1 = 2\nu_r$: The optimum pulse length was found to be $0.2\tau_r$.
- $\nu_1 > 2\nu_r$: The best decoupling was observed when $\tau_p \approx \tau_r$. These optimum pulse length values match with the earlier findings [21].

(iii) XiX: The pulse length was optimised in the range of $\tau_p = 0.1\tau_r$ to $\tau_p = 3.5\tau_r$ and the optimal value was found to be $\tau_p \approx 2.85\tau_r$, which is the recommended pulse length for $\nu_1 > \nu_r$ [22].

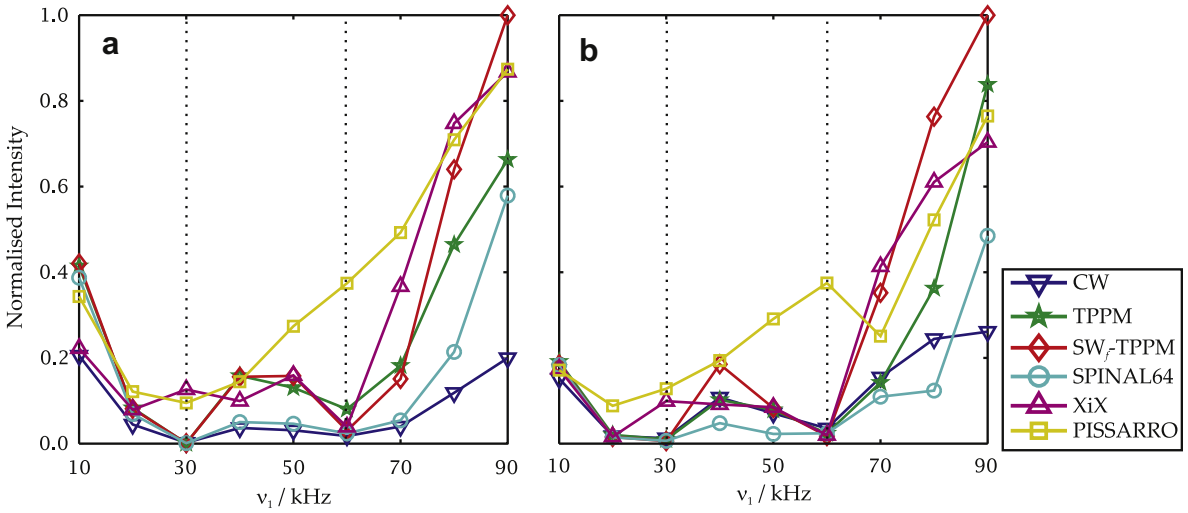

Fig. 2. Intensity comparison of the heteronuclear dipolar decoupling sequences, CW, TPPM, SW_f-TPPM, XiX, SPINAL-64, and PISSARRO as a function of RF amplitude ($10\ \text{kHz} \leqslant \nu_1 \leqslant 90\ \text{kHz}$) at a spinning frequency of 30 kHz. The normalised intensity of the $^{13}CH_2$ peak of a U-^{13}C-glycine sample is plotted. The normalisation was done with respect to the best intensity obtained in the respective cases. The vertical line (dotted) indicates the RR conditions $\nu_1 = \nu_r$ (left) and $\nu_1 = 2\nu_r$ (right) on each plots.

From the data it can be seen that PISSARRO is the only sequence among SW_f-TPPM, TPPM, SPINAL-64, XiX, and CW (see later for a comparison with high-phase TPPM) which does not suffer from heteronuclear dipolar recoupling at the rotary resonance conditions. The data also shows that in the range $\nu_r < \nu_1 < 2\nu_r$, PISSARRO is the suitable sequence for decoupling while above or below these rotary resonance conditions SW_f-TPPM is the suitable choice for heteronuclear dipolar decoupling. The experiments were done on the higher field to investigate the effect of increased CSA. It is seen that the trend for different regions of decoupling remains the same for the different sequences. This suggests that the contribution from the CSA towards the higher-order cross-terms is minimal at the high MAS frequencies.

The above sequences were also applied on a sample of U-^{13}C-L-histidine·HCl·H_2O to check the efficiency of decoupling on a sample which has a large isotropic chemical-shift range for the protons. The decoupling conditions were kept the same as that of U-^{13}C-glycine. The intensity of four peaks of U-^{13}C-L-histidine·HCl·H_2O were monitored as a function of RF amplitude. The four peaks whose intensity are shown in Fig. 3 are (a) CH_2^{β}, (b) CH^{α}, (c) CH^5, and (d) carbonyl carbon. From the plots it is observed that in the region $\nu_1 < \nu_r$ for CH_2^{β} and CH^{α} carbon the best decoupling is achieved with SW_f-TPPM, TPPM, PISSARRO, and SPINAL-64. For the aromatic carbon or the carbonyl carbon, however, the performance of XiX becomes much better and comparable to that of SW_f-TPPM, SPINAL-64, and PISSARRO. In the region $\nu_r < \nu_1 < 2\nu_r$, however, PISSARRO is the sequence of choice because it does not suffer from rotary resonance recoupling. When the RF amplitude is such that $\nu_1 > 2\nu_r$, for the CH_2^{β} and CH^{α} carbon, SW_f-TPPM and PISSARRO deliver the best decoupling. For the other two carbons, however, XiX seems to deliver the best decoupling. From the data it seems that when the proton environment is diluted XiX performs better than most of the sequences. On the other hand in presence of strong homonuclear couplings, SW_f-TPPM does the job better than most of the other sequences.

3.2. Decoupling at the rotary resonance conditions

Recently we introduced a modified version of TPPM for efficient decoupling at the rotary resonance (RR) conditions. The modifications introduced to the basic TPPM unit are (a) the flip angle of the pulse is smaller than that of the conventional TPPM and (b) phase difference between the two pulses is high (≈150°) (compared to ≈30° in conventional TPPM). We refer to this scheme as high-phase TPPM. As the flip angle has a linear dependence on the RF amplitude, the pulse length for high-phase TPPM unit ($\tau_p^{\phi}\tau_p^{-\phi}$) becomes constant ($\tau_p = \frac{\beta}{\nu_1}$). For the set of experiments reported here, it was observed that the pulse length needs to be optimised in the narrow range of 4–6 μs which makes the sequences easy to set up. The phase difference was also optimised and seen to give the best performance when it is ≈150°. We compare the decoupling efficiency of this sequence to that of PISSARRO as it is the only other sequence capable of decoupling at the RR conditions. In the experiments reported here, the optimal pulse duration τ_p of PISSARRO in terms of the rotor period τ_r, $\frac{\tau_p}{\tau_r}$, was found to be in the range of 0.2–0.4.

We have already presented the spectra of U-^{13} C-glycine at the two rotary resonance conditions $\nu_1 = \nu_r$ and $\nu_1 = 2\nu_r$ for two different spinning frequencies [19]. Here, we show the variation of the intensity of the CH_2 resonance of glycine as a function of RF amplitude for the three different sequences, TPPM, PISSARRO, and high-phase TPPM followed by spectra of U-^{13}C-L-histidine·HCl·H_2O acquired using PISSARRO and high-phase TPPM decoupling at the rotary resonance condition $\nu_1 = \nu_r = 30$ kHz, and $\nu_1 = \nu_r = 60$ kHz in Fig. 5. Fig. 4 shows the variation in intensity for the $^{13}CH_2$ peak of U-^{13}C-glycine as a function of RF amplitude ($10\ \text{kHz} \leqslant \nu_1 \leqslant 90\ \text{kHz}$). The data is shown for two different magnetic fields, 500 MHz (left) and 700 MHz (right) in order to verify whether the increased value of the CSA tensor has any effect on the efficiency of decoupling. The plots show that TPPM suffers from heteronuclear recoupling at the RR conditions whilst PISSARRO is efficient in quenching the RR conditions. High-phase TPPM shows a somewhat complementary profile to that of normal TPPM and delivers a better performance than PISSARRO around the $n = 1$ RR condition. The trend remains the same at the higher field too.

Fig. 5 shows the comparison between PISSARRO and high-phase TPPM at MAS frequency of 30 kHz and $\nu_1 = \nu_r$ and $\nu_1 = 2\nu_r$ RR conditions. The spectrometer frequency for ^{1}H was 500 MHz. The ^{13}C resonances of U-^{13}C-L-histidine·HCl·H_2O are plotted in the figure. Fig. 6 has the results at a ^{1}H resonance frequency of 700 MHz. The better efficiency of the high-phase TPPM over PISSARRO is evident from these figures. Fig. 6 further emphasises on the fact that, at high magnetic fields, with the increase of chemical-shift

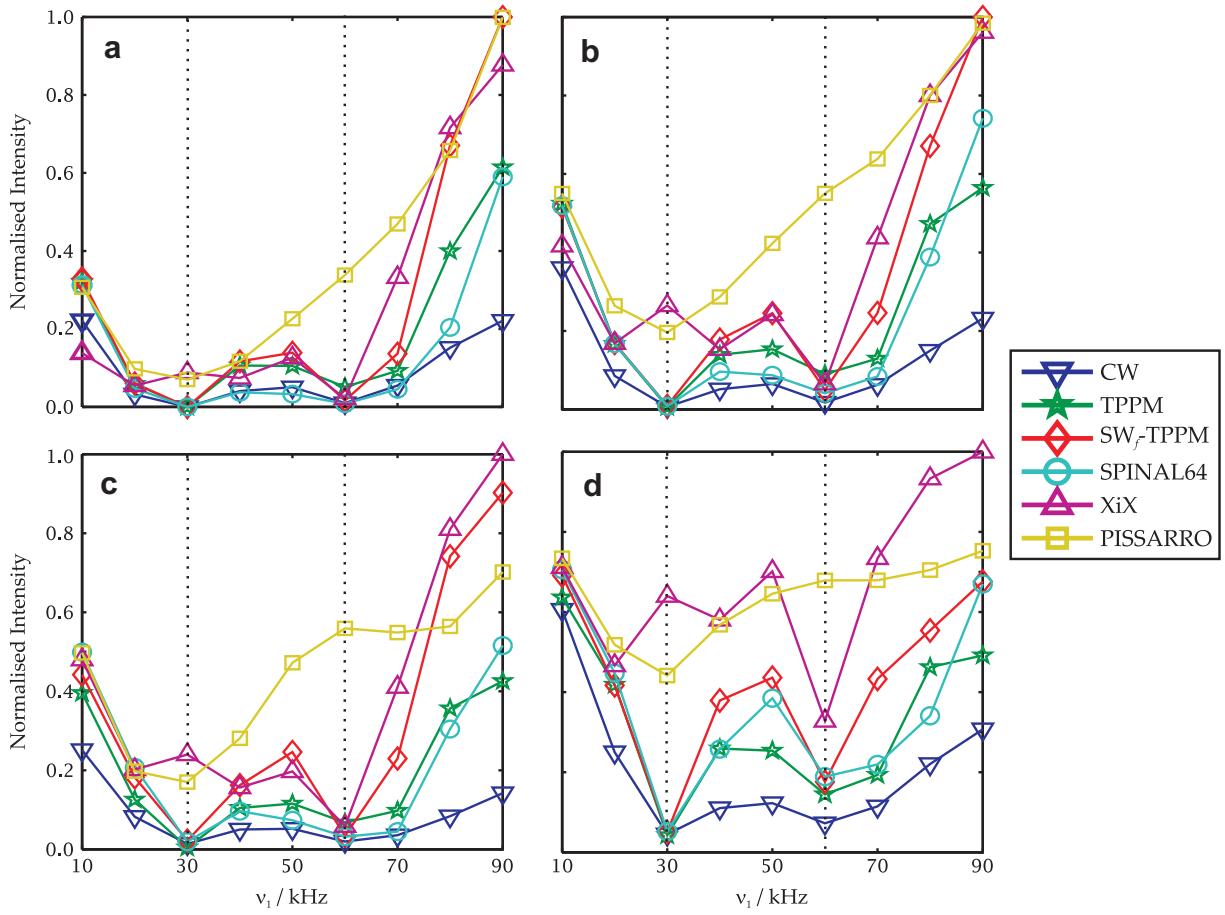

Fig. 3. Intensity comparison of the heteronuclear dipolar decoupling sequences, CW, TPPM, SW_f-TPPM, XiX, SPINAL-64, and PISSARRO as a function of RF amplitude ($10\ \text{kHz} \leqslant \nu_1 \leqslant 90\ \text{kHz}$) at a spinning frequency of 30 kHz. The normalised intensity of (a) CH_2^{β}, (b) CH^{α}, (c) CH^{5}, and (d) carbonyl carbon is plotted. The normalisation was done with respect to the best intensity obtained in the respective cases. The vertical line (dotted) indicates the RR conditions $\nu_1 = \nu_r$ (left) and $\nu_1 = 2\nu_r$ (right) on each plots.

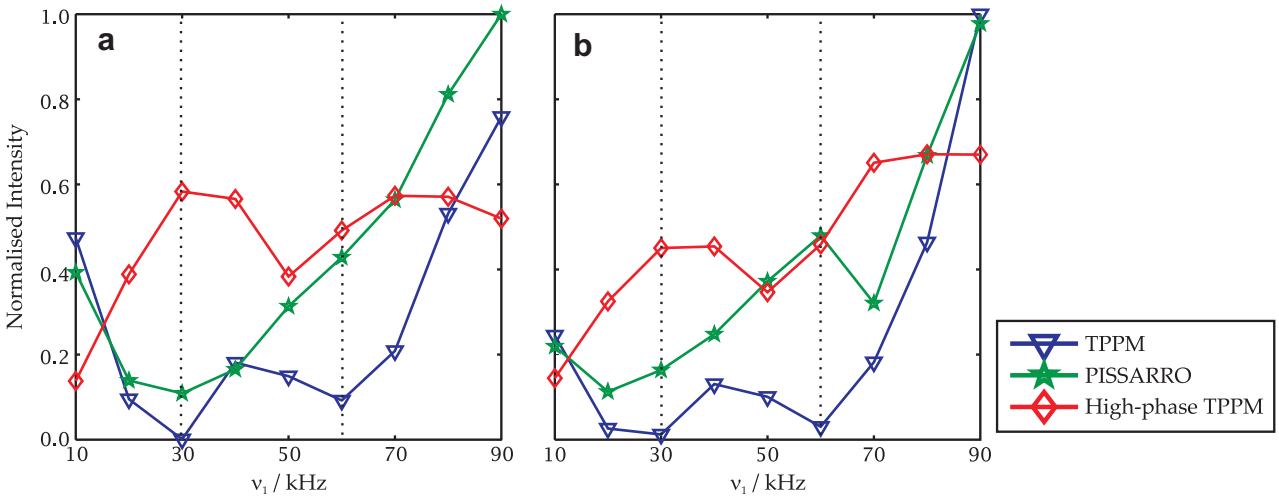

Fig. 4. The normalised intensity of the $^{13}CH_2$ peak of U-^{13}C-glycine as a function of RF amplitude ($10\ \text{kHz} \leqslant \nu_1 \leqslant 90\ \text{kHz}$) at $\nu_r = 30$ kHz for TPPM, PISSARRO, and high-phase TPPM. The vertical line (dotted) indicates the RR conditions $\nu_1 = \nu_r$ (left) and $\nu_1 = 2\nu_r$ (right) on each plots.

anisotropy value, the performance of the high-phase TPPM is still better than PISSARRO at $n = 1$ condition and almost the same at $n = 2$ condition.

Fig. 7 shows the offset dependence of the decoupling efficiency for both the sequences. The RF carrier on the ^{1}H is varied in the range of 2 kHz on either side of on resonance and the intensity for the (a) COO^- peak and (b) $^{13}CH_2$ peak is monitored. From the figures it can be concluded that PISSARRO is more robust than high-phase TPPM with respect to the offset on the ^{1}H. This can be a result of supercycling which leads to better averaging of higher-order cross terms between CSA and heteronuclear dipolar couplings in case of PISSARRO.

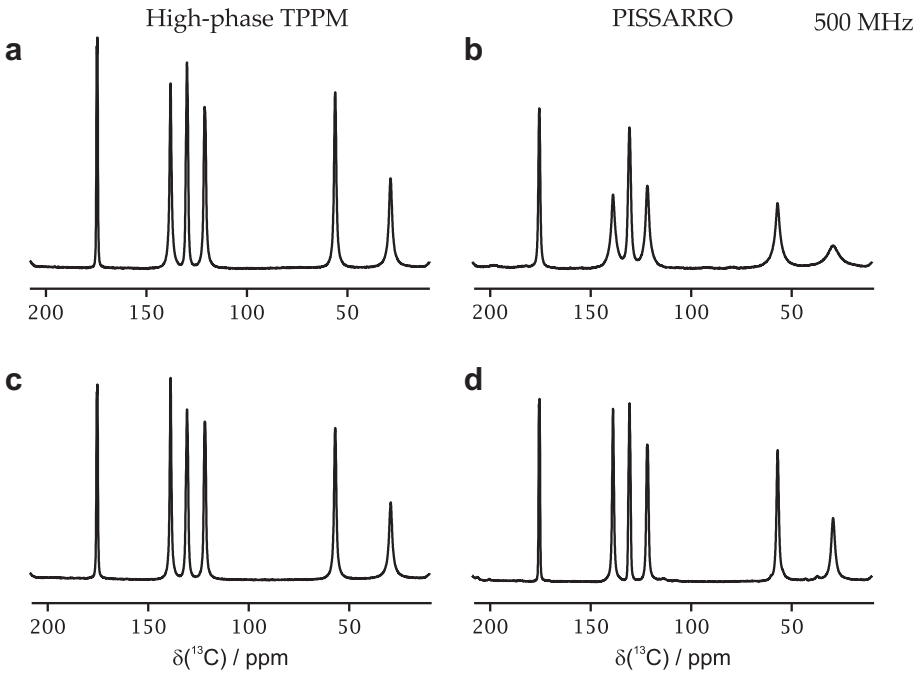

Fig. 5. Spectral comparison of the high-phase TPPM (left panel) and PISSARRO (right panel) observing the ^{13}C resonances of uniformly labelled U-^{13}C-L-histidine·HCl·H_2O (a) $\nu_1 = \nu_r = 30$ kHz (b) $\nu_1 = \nu_r = 30$ kHz (c) $\nu_1 = 2\nu_r = 60$ kHz, and (d) $\nu_1 = 2\nu_r = 60$ kHz. The pulse durations in the case of TPPM were (a) 5.4 μs and (c) 4.5 μs. For PISSARRO the optimum pulse durations were (b) $0.4\tau_r$ and (d) $0.2\tau_r$.

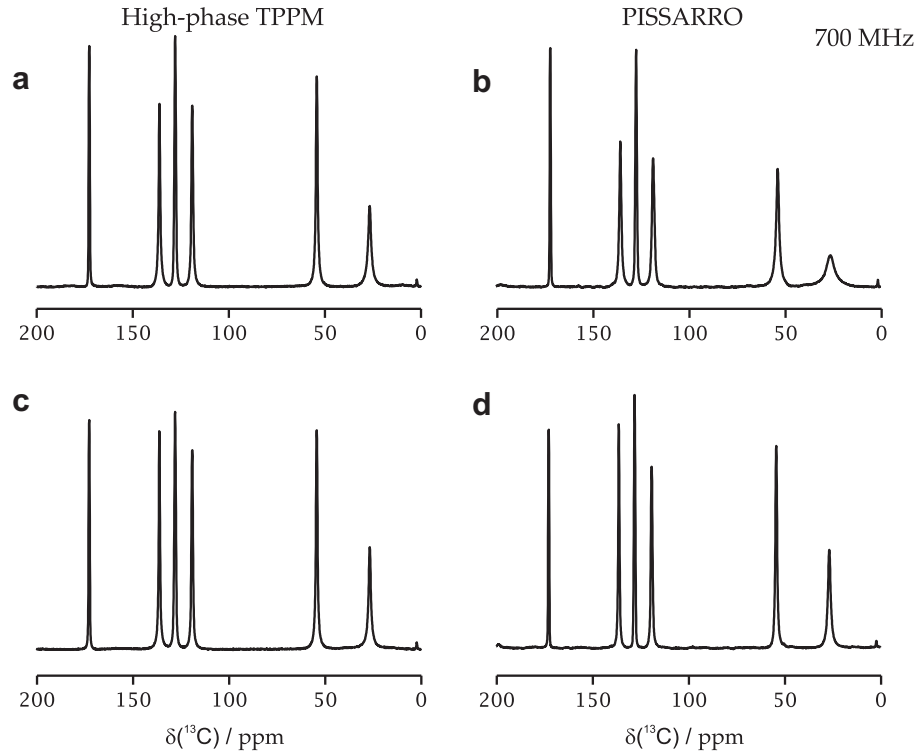

Fig. 6. Spectral comparison of the high-phase TPPM (left panel) and PISSARRO (right panel) observing the ^{13}C resonances of uniformly labelled U-^{13}C-L-histidine·HCl·H_2O (a) $\nu_1 = \nu_r = 30$ kHz (b) $\nu_1 = \nu_r = 30$ kHz (c) $\nu_1 = 2\nu_r = 60$ kHz, and (d) $\nu_1 = 2\nu_r = 60$ kHz. The pulse durations in the case of TPPM were (a) 5.2 μs, and (c) 4.5 μs. For PISSARRO the optimum pulse durations were (c) $0.4\tau_r$ and (d) $0.2\tau_r$.

Fig. 8 shows the simulated intensity variation of the ^{13}C peak of a $^{13}CH_2$ system as a function of homonuclear dipolar coupling strength between the two ^{1}H spins. Fig. 8a shows the simulated intensity variation at $\nu_1 = \nu_r$ for both high-phase TPPM (solid line) and PISSARRO (dashed line) whilst the same is shown for $\nu_1 = 2\nu_r$ in Fig. 8b. PISSARRO at both $n = 1$ and 2 conditions show the trend which is a characteristic for heteronuclear decoupling sequences i.e. the intensity drops with the increase of homonuclear coupling strength [10]. For high-phase TPPM however, the intensity decreases at $n = 1$ condition but remains almost constant at $n = 2$

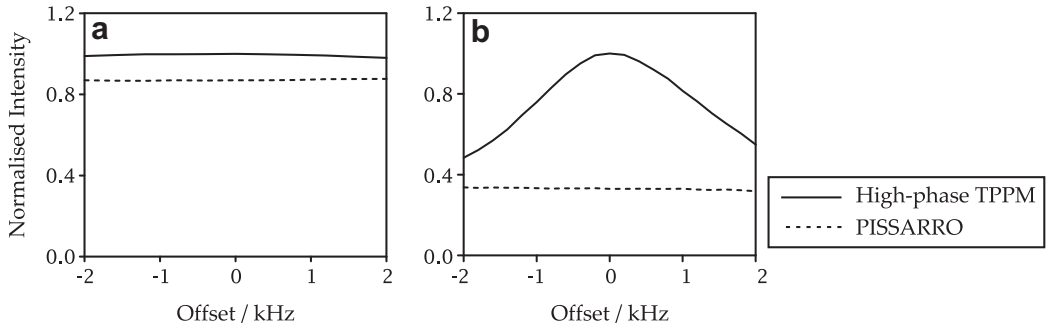

Fig. 7. Intensity variation for (a) COO^- and (b) CH_2peak of U-^{13}C-glycine as a function of the offset on ^{1}H at $\nu_1 = \nu_r = 30$ kHz. For PISSARRO the intensity variation is shown by dotted line whilst for high-phase TPPM it is shown by the solid line. The intensities are normalised to the best intensity obtained in the respective cases.

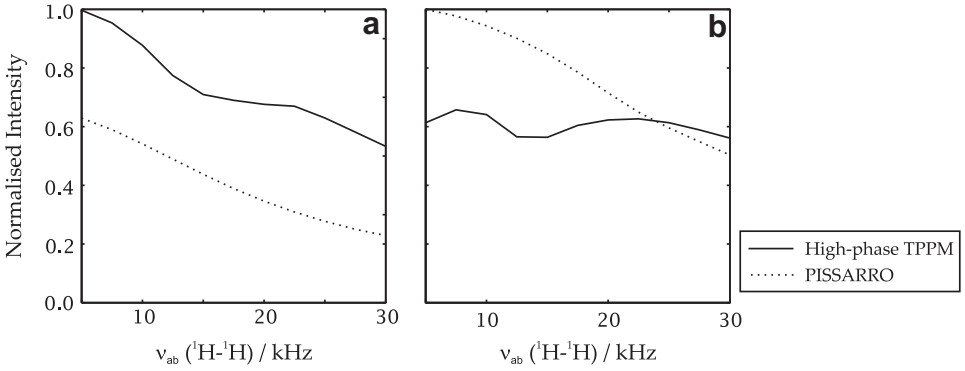

Fig. 8. Simulated intensity variation of the ^{13}C peak of a ^{13} CH_2system as a function of homonuclear dipolar coupling strength between the two ^{1}H spins at (a) $\nu_1 = \nu_r = 30$ kHz and (b) $\nu_1 = 2\nu_r = 60$ kHz for high-phase TPPM (solid line) and PISSARRO (dotted line). The intensity was normalised to the best intensity obtained using high-phase TPPM at $n = 2$ condition. The simulations were done using SPINEVOLUTION [23] as a function of the homonuclear coupling strength between the two protons (5 kHz $\leqslant \nu_{ab} \leqslant$ 30 kHz). The proton Larmor frequency was kept at 500 MHz. ZCW scheme of powder averaging [24–26] with 610 pair of crystallite orientations was employed.

condition. This can be attributed to better homonuclear decoupling rendered with high-phase TPPM at higher RF powers. The homonuclear decoupling abilities of these sequences will be discussed in the next section.

3.3. Properties of high-phase tppm

In this section we discuss some of the properties of the high-phase TPPM sequence. As mentioned earlier the flip angle of this sequence has a linear dependence on the RF amplitude. We plot here the optimum flip angle as a function of RF amplitude at a fixed MAS frequency. The MAS frequency is kept at 30 kHz whilst the RF amplitude is varied from 10 kHz to 90 kHz. The flip angle for the best achievable decoupling is plotted for two different magnetic fields (^{1}H Larmor frequency of 500 MHz and 700 MHz) and the plots confirm the linear dependence. To confirm our observation some simulations were also done using SPINEVOLUTION [23]. The simulated intensity variation of the $^{13}CH_2$ resonance of a $^{13}CHH_2$ fragment as a function of RF amplitude (ν_1) and pulse length (τ_p) at a fixed spinning frequency ($\nu_r = 30$ kHz) is shown in Fig. 9b. The region inside the box is where we optimise the pulse length of the high-phase TPPM unit during the experiments. The contours clearly show that the region inside the box is the best decoupling region. This corroborates with the experimental findings and simplifies the applicability of the sequence to a great extent as the pulse length can be kept fixed at around 5 μs at all the RF amplitudes at a fixed spinning frequency.

To understand the properties of high-phase TPPM decoupling we report some simulations in the presence and absence of homonuclear couplings. The simulated intensity variation of the ^{13}C resonance of a $^{13}CHH_2$ fragment as a function of RF amplitude (ν_1) and pulse length (τ_p) at RR condition of $n = 1$ is shown in Fig. 10. The left panel shows the simulation data in the absence of homonuclear couplings whilst the right panel shows the simulation data in the presence of homonuclear couplings. The plots are quite different from the conventional decoupling sequences where presence of homonuclear couplings broadens out the regions of good decoupling [10]. From the two plots shown here it is evident that the presence of homonuclear couplings does not affect the heteronuclear dipolar decoupling at the RR conditions.

It is known that the appearance of ^{1}H-^{13}C J-splitting of ^{13}C peaks of adamantane is an indication of homonuclear decoupling. So in order to check the homonuclear decoupling capabilities of high-phase TPPM and PISSARRO, ^{1}H–^{13}C J-splitting of ^{13}C peaks of adamantane was observed at $\nu_r = \nu_1 = 30$ kHz using both the decoupling sequences. The plots shown in Fig. 11 show that both these sequences have some homonuclear decoupling capabilities at the RR condition.

The effective field on the ^{1}H for both (c) high-phase TPPM and (d) PISSARRO is shown in the bottom panel of Fig. 11. The effective field calculation was done by calculating the propagator after a unit of TPPM or PISSARRO. The propagator calculation was done by taking a single ^{1}H spin in SPINEVOLUTION and observing the propagator after applying the decoupling sequences and acquiring one point. The form of the propagator then gives the effective field and the flip angle induced on the ^{1}H spin.

The J-splitting patterns in Fig. 11 indicate that PISSARRO is a better sequence in the sense of homonuclear decoupling capability but it does not perform as well as high-phase TPPM in the heteronuclear dipolar decoupling scenario. This implies that homonuclear decoupling is not the only criterion for the heteronuclear dipolar decoupling at the RR conditions. Further theoretical

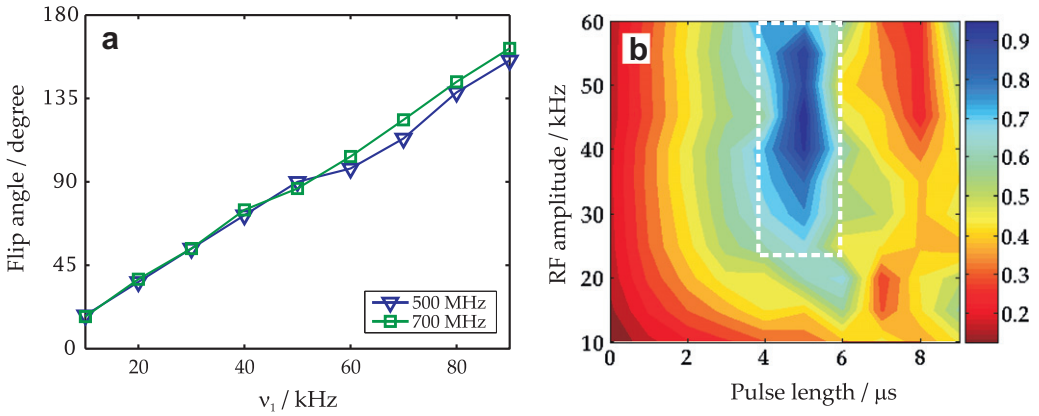

Fig. 9. (a) The optimum flip angle for the high-phase TPPM sequence as a function of RF amplitude for two different spectrometers operating at the proton Larmor frequencies of 500 MHz and 700 MHz. (b) Contour plot showing the intensity of a $^{13}CHH_2$ system obtained with SPINEVOLUTION programme as a function of the pulse duration and $\nu_1 = \nu_r = 30$ kHz for high-phase TPPM. The isotropic chemical-shift separation between the H and the H_2 system was 2 ppm and the irradiation frequency on the protons was kept on resonance. The fragment has a dipolar coupling strength of 22 kHz between ^{13}C and two of the protons and 10 kHz with the other proton. The simulations were done with the ZCW scheme of powder averaging [24–26] with 610 pair of crystallite orientations. The CSA of the protons are kept at 1 kHz. The homonuclear dipolar coupling constant between one of the H in H_2 and H was −23.3 kHz, the second H in H_2 and H was −8.4 kHz, and between the two H in H_2 was −8.6 kHz.

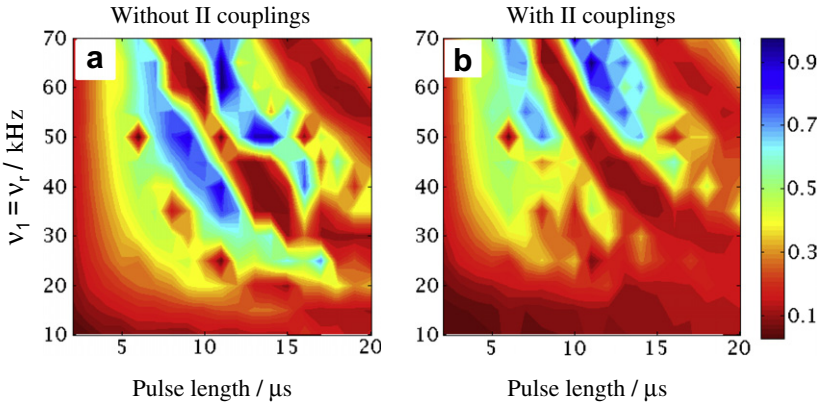

Fig. 10. Contour plots showing the intensity of a $^{13}CHH_2$ system obtained with SPINEVOLUTION programme as a function of the pulse duration and ν_1 at $\nu_r = 30$ kHz for high-phase TPPM (a) without II couplings and (b) with II couplings. The isotropic chemical-shift separation between the H and the H_2 system was 2 ppm and the irradiation frequency on the protons was kept on resonance. The fragment has a dipolar coupling strength of 22 kHz between ^{13}C and two of the protons and 10 kHz with the other proton. The simulations were done with the ZCW scheme of powder averaging [24–26] with 610 pair of crystallite orientations. The CSA of the protons are kept at 1 kHz. The homonuclear dipolar coupling constant between one of the H in H_2 and H was −23.3 kHz, the second H in H_2 and H was −8.4 kHz, and between the two H in H_2 was −8.6 kHz.

investigations are being pursued to understand the effect of homonuclear and heteronuclear couplings at the RR conditions and to justify why these sequences are successful in decoupling at the otherwise heteronuclear recoupling conditions.

4. Choice of decoupling sequences

One of the concerns for an experimentalist is the choice of the decoupling sequence at a given MAS frequency and RF amplitude. Fig. 12 addresses this issue gathering together experimental results of the present work and earlier reports [7,10–13,16,18,19,21].

The plot can be divided into five regions in terms of RF amplitude at a certain spinning frequency. The five regions are as follows:

- $\nu_1 < \frac{\nu_r}{2}$
- $\frac{\nu_r}{2} \leqslant \nu_1 < 2\nu_r$
- $\nu_1 = 2\nu_r$
- $2\nu_r < \nu_1 < 3\nu_r$
- $\nu_1 \geqslant 3\nu_r$

In the first region it is found that SW_f-TPPM and TPPM deliver the best performance. The second region is predominantly the heteronuclear recoupling region where the sequences which are able to quench the RR conditions, PISSARRO and high-phase TPPM, are the only ones which can be used. As high-phase TPPM delivers a better performance compared to PISSARRO at this region, the former can be used in this region. At the second RR condition which is the third region both high-phase TPPM and PISSARRO give similar performance and either one can be used. At the fourth region PISSARRO performs better than the other sequences whilst at the high power, i.e. the fifth region, SW_f-TPPM is found to perform better than the other sequences and more robust with respect to offresonance and cycle frequency and much easier to optimise than the other sequences.

We also indicate the percentage of intensity that can be recovered at $\nu_r = 30$ kHz using the sequence of choice at the five regions mentioned above. From the data following conclusions can be drawn:

(a) The percentage of intensity that can be recovered at the rotary resonance conditions is almost 50% to that of the intensity recovered at moderately high RF amplitude of 100 kHz.
(b) The decoupling becomes better at higher RF amplitudes of $\nu_1 > 4\nu_r$.

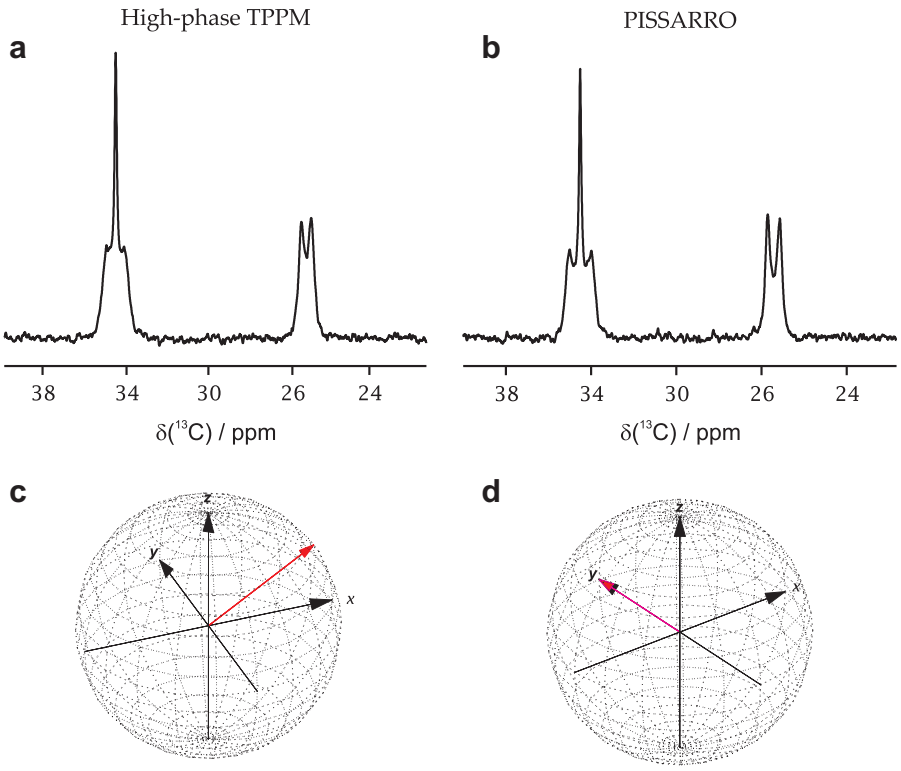

Fig. 11. ^{1}H–^{13}C *J*-splitting of the ^{13}C peaks of adamantane observed using (a) high-phase TPPM, and (b) PISSARRO decoupling at $\nu_r = \nu_r = 30$ kHz. For high-phase TPPM the carrier was kept at −6 kHz whilst for PISSARRO it was kept at −2 kHz from the center of the proton spectra. (c) and (d) show the effective field direction on ^{1}H for high-phase TPPM and PISSARRO respectively. The effective field is shown by the red arrow where the polar angle (θ) and the azimuthal angle (ϕ) are found to be (c) $\theta = 58.4923°$ and $\phi = 0°$, and (d) $\theta = 90°$ and $\phi = 90°$.

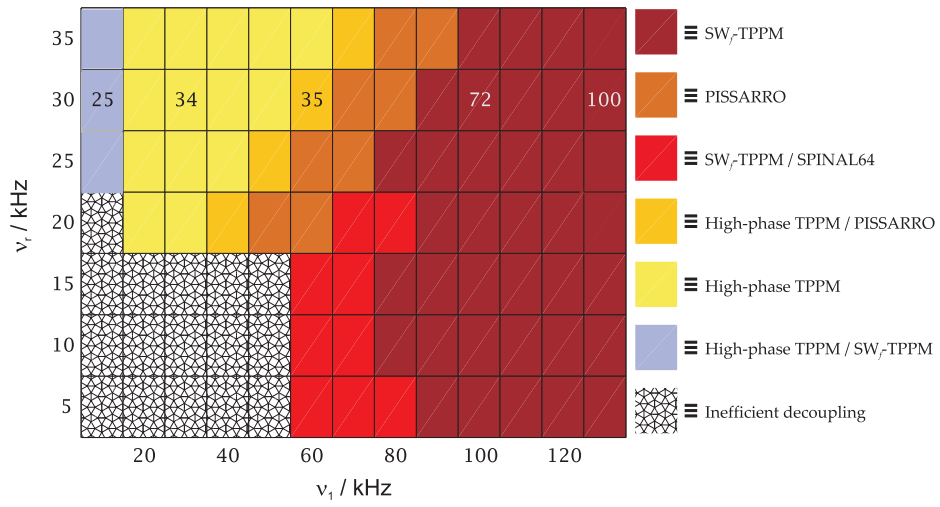

Fig. 12. A plot showing the best decoupling sequence as a function of RF amplitude (ν_1) and MAS frequency (ν_r). Percentage of intensity recovered utilising the heteronuclear decoupling of choice is also indicated on the figure at 30 kHz of spinning frequency. The data was collected at the proton Larmor frequency of 700 MHz.

(c) The intensity recovered at the lowest RF regime is about 35% to that of the moderate high RF amplitude ($\nu_1 = 100$ kHz) and 25% to that of the very high RF amplitudes $\nu_1 > 4\nu_r$.

5. Conclusions

We have presented here a comparison of heteronuclear dipolar decoupling sequences at a moderate spinning frequency of 30 kHz. The decoupling efficiency of the different sequences was investigated as a function of RF amplitude which was scanned from 5 kHz to 90 kHz including the RR conditions. The studies have shown that SW_f-TPPM is the sequence of choice at high power decoupling $\nu_1 > 2\nu_r$ whilst TPPM and SW_f-TPPM perform better than the other decoupling sequences at low power $\nu_1 < \nu_r$. The emphasis is mainly on the decoupling at the RR conditions where high-phase TPPM is found to be the sequence of choice. We have presented some of the properties of the high-phase TPPM sequence which make the sequence easily applicable. Further we have

discussed homonuclear dipolar decoupling with PISSARRO and high-phase TPPM which may help us understand decoupling at the heteronuclear recoupling conditions.

Acknowledgments

We acknowledge the National Facility for High Field NMR, TIFR, Mumbai, and technical assistance of M.V. Naik.

References

[1] A.L. Bloom, J.N. Shoolery, Effects of perturbing radiofrequency fields on nuclear spin coupling, Phys. Rev. 97 (1955) 1261.
[2] A.E. Bennett, C.M. Rienstra, M. Auger, K.V. Lakshmi, R.G. Griffin, Heteronuclear decoupling in rotating solids, J. Chem. Phys. 103 (1995) 6951.
[3] Z.H. Gan, R.R. Ernst, Frequency- and phase-modulated heteronuclear decoupling in rotating solids, Solid State Nucl. Magn. Reson. 8 (1997) 153.
[4] K. Takegoshi, J. Mizokami, T. Terao, ^{1}H decoupling with third averaging in solid NMR, Chem. Phys. Lett. 341 (2001) 540.
[5] B.M. Fung, A.K. Khitrin, K. Ermolaev, An improved broadband decoupling sequence for liquid crystals and solids, J. Magn. Reson. 142 (2000) 97.
[6] G.D. Paëpe, D. Sakellariou, P. Hodgkinson, S. Hediger, L. Emsley, Heteronuclear decoupling in NMR of liquid crystals using continuous phase modulation, Chem. Phys. Lett. 368 (2003) 511.
[7] R.S. Thakur, N.D. Kurur, P.K. Madhu, A Swept-frequency two-pulse phase modulation for heteronuclear dipolar decoupling in solid-state NMR, Chem. Phys. Lett. 426 (2006) 459.
[8] C.V. Chandran, P.K. Madhu, N.D. Kurur, T. Bräuniger, Swept-frequency two-pulse phase modulation (SW_f-TPPM) sequences with linear sweep profile for heteronuclear decoupling in solid-state NMR, Magn. Reson. Chem. 46 (2008) 943.
[9] C.V. Chandran, T. Bräuniger, Efficient heteronuclear dipolar decoupling in solid-state NMR using frequency-swept SPINAL sequences, J. Magn. Reson. 200 (2009) 226.
[10] M. Leskes, R.S. Thakur, P.K. Madhu, N.D. Kurur, S. Vega, Bimodal Floquet description of heteronuclear dipolar decoupling in solid-state nuclear magnetic resonance, J. Chem. Phys. 127 (2007) 024501.
[11] R.S. Thakur, N.D. Kurur, P.K. Madhu, An analysis of phase-modulated heteronuclear dipolar decoupling sequences in solid-state nuclear magnetic resonance, J. Magn. Reson. 193 (2008) 77.
[12] R.S. Thakur, N.D. Kurur, P.K. Madhu, Pulse duration and phase modulated heteronuclear dipolar decoupling schemes in solid-state NMR, Proc. Ind. Nat. Sci. Acad., Springer Verlag, 2009.
[13] R.S. Thakur, N.D. Kurur, P.K. Madhu, An experimental study of decoupling sequences for multiple-quantum and high-resolution MAS experiments in solid-state NMR, Magn. Reson. Chem. 46 (2008) 166.
[14] M. Ernst, A. Samoson, B.H. Meier, Low-power decoupling in fast magic-angle spinning NMR, Chem. Phys. Lett. 348 (2001) 293.
[15] M. Ernst, A. Samoson, B.H. Meier, Low-power XiX decoupling in MAS NMR experiments, J. Magn. Reson. 163 (2003) 332.
[16] M. Kotecha, N.P. Wickramasinghe, Y. Ishii, Efficient low-power heteronuclear decoupling in ^{13}C high-resolution solid-state NMR under fast magic angle spinning, Magn. Reson. Chem. 45 (2007) S221.
[17] T.G. Oas, R.G. Griffin, M.H. Levitt, Rotary resonance recoupling of dipolar interactions in solid-state nuclear magnetic resonance spectroscopy, J. Chem. Phys. 89 (1988) 692.
[18] M. Weingarth, P. Tekely, G. Bodenhausen, Efficient heteronuclear decoupling by quenching rotary resonance in solid-state NMR, Chem. Phys. Lett. 466 (2008) 247.
[19] S. Paul, V.S. Mithu, N.D. Kurur, P.K. Madhu, Heteronuclear dipolar decoupling in solid-state nuclear magnetic resonance at rotary resonance conditions, J. Magn. Reson. 203 (2010) 199.
[20] M. Ernst, Heteronuclear spin decoupling in solid-state NMR under magic-angle sample spinning, J. Magn. Reson. 162 (2003) 1.
[21] M. Weingarth, G. Bodenhausen, P. Tekely, Low-power decoupling at high spinning frequencies in high static fields, J. Magn. Reson. 199 (2009) 238.
[22] A. Detken, E.H. Hardy, M. Ernst, B.H. Meier, Simple and efficient decoupling in magic-angle spinning solid-state NMR: the XiX scheme, Chem. Phys. Lett. 356 (2002) 298.
[23] M. Veshtort, R.G. Griffin, SPINEVOLUTION: a powerful tool for the simulation of solid and liquid state NMR experiments, J. Magn. Reson. 178 (2006) 248.
[24] S.K. Zaremba, Good lattice points, discrepancy, and numerical integration, Ann. Mat. Pura Appl. 293 (1966) 4.
[25] H. Conroy, Molecular Schrödinger equation. VIII. A new method for the evaluation of multidimensional integrals, J. Chem. Phys. 47 (1967) 5307.
[26] V.B. Cheng, H.H. Suzukawa Jr., M. Wolfsberg, Investigations of a nonrandom numerical method for multidimensional integration, J. Chem. Phys. 59 (1973) 3992.